Delft University of Technology

Temperature-sensing performance of polymer-derived SiAlCN ceramics up to 1000 °C

Shao, Pengfei; Ma, Chao; Han, Daoyang; Liu, Kun; Li, Mingliang; Liang, Yi; Yao, Meng; Wang, Hailong; Zhang, Rui; Shao, Gang

Important note
To cite this publication, please use the final published version (if applicable).
Please check the document version above.

Temperature-sensing performance of polymer-derived SiAlCN ceramics up to 1000 °C

Pengfei Shao [a,1], Chao Ma [a,b,1], Daoyang Han [a], Kun Liu [a], Mingliang Li [a], Yi Liang [a], Meng Yao [a], Hailong Wang [a], Rui Zhang [a,c], Gang Shao [a,*]

[a] *School of Materials Science and Engineering, Zhengzhou University, Zhengzhou, 450001, Henan, People's Republic of China*
[b] *Radiation Science and Technology, Faculty of Applied Science, Delft University of Technology, 2629, JB Delft, Mekelweg 15, the Netherlands*
[c] *School of Materials Science and Engineering, Luoyang Institute of Science and Technology, Luoyang, 471023, Henan, People's Republic of China*

ARTICLE INFO

ABSTRACT

Temperature sensors that can operate in high-temperature and harsh environments are highly desired. However, this is a great challenge for sensing materials to operate under extreme working conditions because of oxidation and/or corrosion at high temperature. In this study, polymer-derived SiAlCN ceramics were prepared as sensing materials to overcome the abovementioned issues. A SiAlCN ceramic temperature sensor was designed and fabricated, and it performed excellent temperature-sensing properties with high accuracy, high stability, and high repeatability up to 1000 °C. Compared with traditional thermocouples, the SiAlCN ceramic sensor exhibited a faster response rate (a shorter response time). These results showed that SiAlCN ceramic is a promising sensor material for temperature measurement in high-temperature and harsh environments.

1. Introduction

Temperature measurement and monitoring are of great significance in many fields, such as biomedical science, the automatic industry, and communication engineering, especially in high-temperature and oxidizing/corrosive environments [1–3]. The aero-engine is a typical example. Real-time temperature monitoring of aero-engines is very important and urgently required, which could improve efficiency, reduce pollution, and monitor engine operating conditions [4]. However, most commercially available temperature sensors have drawbacks in harsh environments. Traditional metal-based thermocouples cannot survive under corrosive and oxidizing conditions, resulting in a short lifespan [5]. Fiber optical sensors have disappointing stability and accuracy, which limit their application in high-temperature environments. Ceramic thermistors show better performance than thermocouples in terms of oxidation/corrosion resistance, but the complicated fabrication method and temperature limitation confine their widespread application [6]. Therefore, it is necessary to explore and develop new sensor materials that can work well in extreme environments.

Polymer-derived ceramics (PDCs) are novel materials obtained by thermal decomposition of polymeric precursors [7]. They have been widely investigated for many application purpose, such as micro-electro-mechanical systems (MEMS) [8], high-temperature sensors [9], microwave absorption [10], and energy storage [11], owing to their excellent high-temperature stability, high-temperature creep resistance [12], oxidation/corrosion resistance [13], negative temperature coefficient of resistance (NTCR) [14] and giant piezoresistive effect [15]. For example, some silicon-based polymer-derived ceramics, such as SiC, have been used to develop temperature sensors, but their low operating temperature (lower than 600 °C) and poor oxidation resistance limit their application in extreme high-temperature environments [16]. It has been demonstrated that the high-temperature operation of polymer-derived ceramics can be enhanced by introduction of some alternative elements, such as B, Al, and Fe [17–19]. Wang et al. found that SiAlCN ceramic showed better corrosion/oxidation resistance and high-temperature stability than SiCN ceramic owing to prevention of oxygen diffusion by the aluminum atoms [13,20]. Zhao et al. and Yu et al. found that SiAlCN ceramic exhibited excellent temperature-sensing sensitivity and repeatability (up to 830 °C) [9,21]. Moreover, we have found that the conductive mechanism of SiAlCN ceramic is band-tail hopping rather than variable-range hopping by analyzing the relationship between the conductivity (σ_0) and
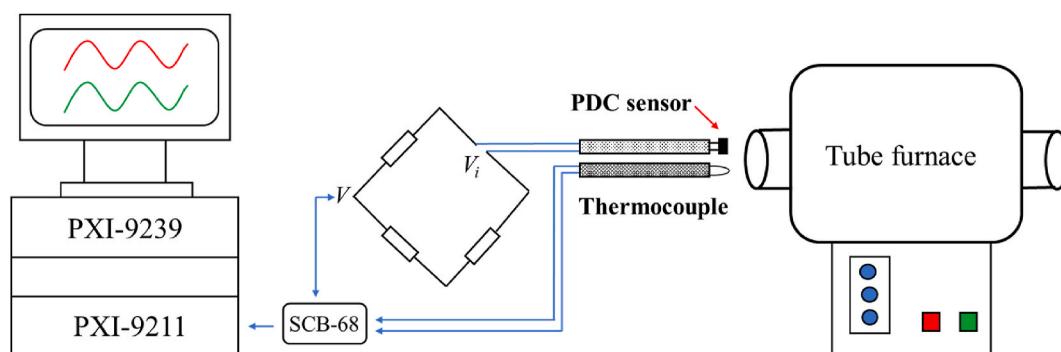

Fig. 1. A schematic diagram of the sensor test platform.

temperature (T_0) [22], indicating that the thermally excited conductivity of SiAlCN ceramic is favorable for high-temperature sensor application. Therefore, SiAlCN ceramic is a promising candidate material for high-temperature sensor application, and the performance of the SiAlCN sensor should be evaluated at higher temperature for a longer time. Though the polymer-derived SiAlCN ceramic sensor has been reported previously, the testing temperature is relatively low (830 °C) [9, 21]. Therefore, sensing performance of SiAlCN ceramic sensor at higher temperature need to be investigated.

In this work, polymer-derived SiAlCN ceramics were synthesized at different pyrolysis temperatures. A SiAlCN ceramic high-temperature sensor was fabricated and its sensing performance, including resistance–temperature characteristics, sensitivity, repeatability and stability, were evaluated by a test system based on a Wheatstone bridge in the temperature range from 25 to 1000 °C. The results revealed that the polymer-derived SiAlCN ceramic is a promising temperature-sensing material for high temperature and harsh environments.

2. Experimental

2.1. Materials

The sensor head was fabricated with polymer-derived SiAlCN ceramic using commercially available polysilazane (PSN−2, Institute of Chemistry, Chinese Academy of Sciences, Beijing, China) and aluminum-tri-*sec*-butoxide (ASB, 97%, Sigma– Aldrich, Shanghai, China) as the precursors. Dicumyl peroxide (DP, 98%, Sigma−Aldrich, Shanghai, China) was used as the thermal initiator.

2.2. Synthesis of the SiAlCN ceramics

The polymer-derived SiAlCN ceramics were synthesized based on our previously reported research [22]. In Brief, 20.0 g PSN and 2.0 g ASB were mixed in a reaction vessel in an ultrahigh-purity N_2 environment. The solution was then mixed under magnetic stirring in an oil bath at 80 °C for 1 h. Subsequently, 1.1 g DP was added to the solution with continuous magnetic stirring at 50 °C for 30 min. The liquid SiAlCN precursor was then cross-linked in a vacuum oven at 140 °C for 3 h to obtain an infusible solid precursor, which was subsequently milled into fine powder of ~1 μm by high-energy ball milling. Finally, the fine powder was uniaxially pressed into discs with diameter of 12 mm and thickness of approximately 2 mm, and the pressed green bodies were pyrolyzed at different temperatures (1000–1400 °C) for 4 h under the protection of ultrahigh purity N_2.

2.3. Characterization

The powder X-ray diffraction (XRD) patterns of the SiAlCN ceramics were recorded with an X-ray diffractometer (SmartLab, Rigaku Instrument Corp., Kyoto, Japan) using monochromatic Cu-Kα radiation with a wavelength of $\lambda/2 = 154.06$ p.m. to study the crystallization behavior of the SiAlCN ceramics. The Raman spectra were recorded with a micro-Raman spectrometer (LabRAM HR Evolution, Horiba Jobin Yvon Co. Ltd., Kyoto, Japan) using the 532 nm line of the silicon-solid laser as the excitation source, to investigate the evolution of the free carbon phase and graphitization. The compositions of all of the samples were measured with a carbon-sulfur analyzer (LECO-CS230, America) for C and an oxygen-nitrogen analyzer (LECO-TC500, America) for N and O. The Al content was measured by inductively coupled plasma atomic emission spectroscopy (ICP-AES-6300, America). The Si content (M_{Si}) was calculated by the following equation:

$$M_{Si} = 1 - M_O - M_C - M_N - M_{Al}$$

2.4. Fabrication of the sensor head

The SiAlCN ceramic pyrolyzed at 1000 °C was used to prepare the temperature sensor head. The pyrolyzed ceramic was cut into a specifically designed size of 6 mm × 5 mm × 1.5 mm as the sensor head. To fabricate electrodes, two holes with a diameter of 0.5 mm were drilled and platinum paste was evenly coated on the inner wall of the two holes. Two platinum wires with a diameter of 0.2 mm were then soldered into the holes with addition of a special prepared solder. The specially prepared solder in this work was the mixture of liquid SiAlCN precursor and the milled powder of cross-linked SiAlCN precursor. Finally, the sensor head was sintered at 850 °C for 10 min to tightly embed the platinum wires inside the sensor body.

2.5. Measurement of sensor performance

The resistance–temperature characteristic ($R-T$ curve) and direct-current (DC) conductivities of the SiAlCN ceramics were measured with a high-temperature resistance measurement system (HRMS-900, Partulab Technology Co. Ltd., China). To evaluate the performance of the SiAlCN temperature sensor, a test platform was built. A schematic diagram of the test platform is shown in Fig. 1. The test system consisted of a data acquisition system and an acquisition module. LabVIEW software was used to collect the output voltage signal of the circuit and temperature signal of the thermocouple. The SiAlCN sensor was connected to a Wheatstone bridge, which is beneficial to improve the sensitivity of the test system. The resistance of the three equivalent arms was 20 KΩ and a K-type thermocouple was used for real-time monitoring of the temperature. The entire circuit was powered by a battery source. To evaluate the repeatability and sensitivity, the SiAlCN sensor and thermocouple were fixed on the mobile platform together. They were heated for 1 min in a tube furnace maintained at 1000 °C and then cooled for 2 min at room temperature. This process was repeated 60 times, and the whole procedure was automatically controlled. To test the stability, the SiAlCN sensor was heated for 5 h at 1000 °C and the
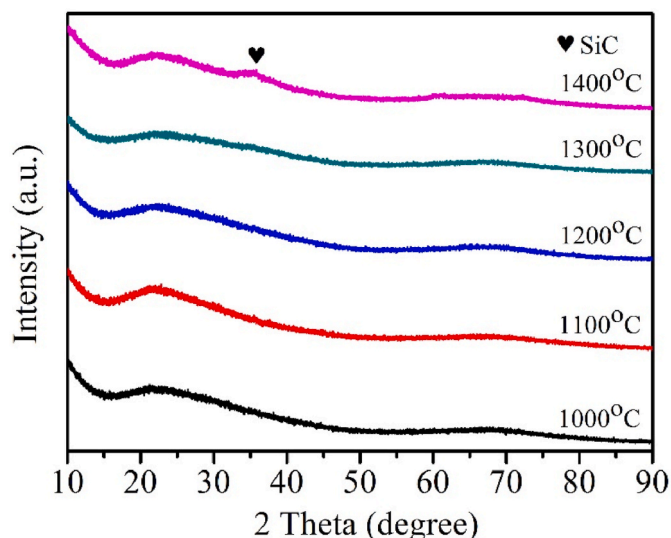
Fig. 2. XRD patterns of the SiAlCN ceramics pyrolyzed at different temperatures.

Table 1
DC conductivities and elemental compositions of the SiAlCN ceramics pyrolyzed at different temperatures.

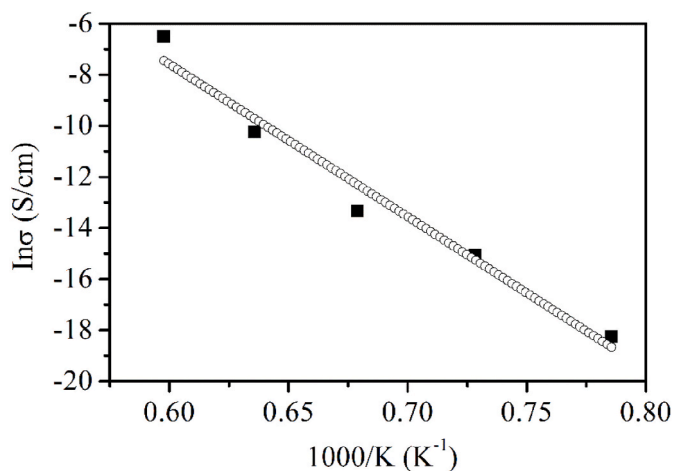| Pyrolysis temperature (°C)	DC conductivity (S/cm)	Atomic ratio
1000	1.19 E−8	$SiAl_{0.03}C_{0.82}N_{0.67}O_{0.3}$
1100	2.90 E−7	$SiAl_{0.03}C_{0.74}N_{0.69}O_{0.34}$
1200	1.62 E−6	$SiAl_{0.03}C_{0.81}N_{0.69}O_{0.3}$
1300	3.58 E−5	$SiAl_{0.03}C_{0.78}N_{0.69}O_{0.3}$
1400	1.50 E−3	$SiAl_{0.03}C_{0.66}N_{0.53}O_{0.3}$

Fig. 3. Conductivity of the SiAlCN ceramic as a function of pyrolysis temperature as an Arrhenius plot.

variation of output voltage was collected by LabVIEW.

The instantaneous output voltage (V_i) was calculated by the following Wheatstone bridge circuit equation:

$$V_i = \frac{R_0 - R_S}{2(R_0 + R_S)} V \tag{1}$$

where R_0 is the fixed resistance, R_s is the resistance of the SiAlCN sensor, and V is the input voltage, which was 10 V in this study.
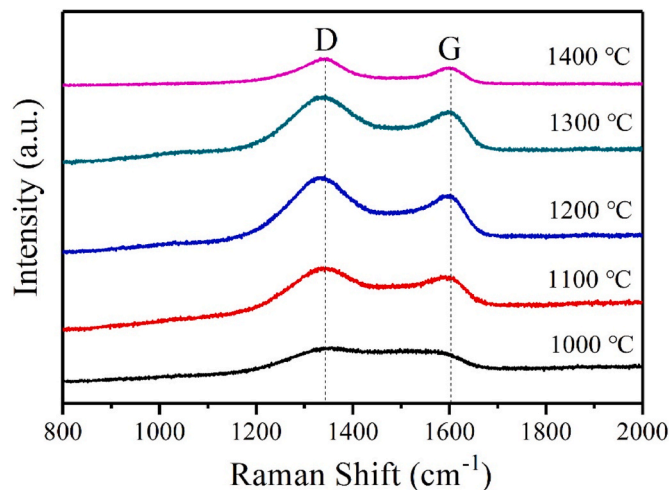

Fig. 4. Raman spectra of the SiAlCN ceramics pyrolyzed at different temperatures.

Table 2
Curve fitting data of Raman spectra with different pyrolysis temperatures.

Pyrolysis temperature (°C)	1000	1100	1200	1300	1400
D peak position (cm^{-1})	1350	1342	1333	1339	1337
G peak position (cm^{-1})	1540	1581	1590	1592	1600
FWHM (D peak)	166	151	139	142	106
FWHM (G peak)	175	129	111	104	71
I_D/I_G	1.01	1.40	1.42	1.52	1.69
L_a (nm)	1.28	1.50	1.51	1.57	1.65

3. Results and discussion

3.1. Characterization of the SiAlCN ceramics

Powder XRD was performed to investigate crystallization of the SiAlCN ceramics. The XRD patterns of the SiAlCN ceramics calcined at different temperatures are shown in Fig. 2. All of the XRD patterns showed broad peaks at 15°–30°, suggesting that the prepared ceramics were typically amorphous solids. There was a weak peak at approximately 35° for the SiAlCN ceramic pyrolyzed at 1400 °C, which originated from the (111) plane of β−SiC [23]. The DC electrical conductivities and elemental compositions of the polymer-derived SiAlCN ceramics pyrolyzed at different temperatures are given in Table 1. The elemental composition revealed that the aluminum element was successfully introduced, but a small fraction of oxygen was also present, which was probably caused by ASB. The conductivity of the SiAlCN ceramic increased by five orders of magnitude with increasing pyrolysis temperature. To further analyze the evolution of the conductivity, the relationship between the conductivity of the SiAlCN ceramic and the pyrolysis temperature is plotted in Fig. 3. The results followed the Arrhenius relation and the active energy of the SiAlCN ceramic was estimated to be 5.15 eV, which differs from the value of the SiCN ceramic reported in Ref. [24]. The different active energy may be related to the distinct structure rather than only depending on the evolution of the free carbon phase.

The Raman spectra of the SiAlCN ceramics pyrolyzed at different temperatures are shown in Fig. 4. There were two characteristic peaks in Raman spectra, namely, the D peak at ~1350 cm^{-1} owing to the breathing modes of the sp^2 atoms in rings and the G peak at ~1600 cm^{-1} stemmed from in-plane bond stretching of sp^2 carbon atoms [25–27]. To obtain more detailed structure information, the Raman spectra were curve-fitted for the D peak and G peak using the Lorentzian function and Breit−Wigner−Fano function, respectively. The fitting parameters of
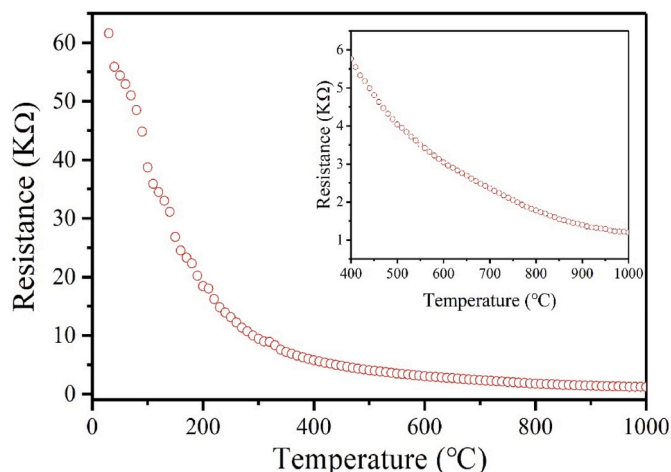
Fig. 5. Resistance of the SiAlCN ceramic pyrolyzed at 1000 °C as a function of temperature.

Fig. 6. Plot of the resistance of the SiAlCN ceramic as a function of temperature in the format of ln (R_t) vs. $1/T$.

the polymer-derived SiAlCN ceramics are given in Table 2. The position of the G peak sharply increased from 1000 °C to 1100 °C and then slowly increased when the pyrolysis temperature continued to increase. The full width at half maximum (FWHM) of the G peak gradually decreased from 174 to 71 with increasing temperature. These results illustrated that the free carbon phase of the SiAlCN ceramic changed from amorphous to nanocrystalline and became more ordered with increasing pyrolysis temperature from 1000 to 1400 °C [28]. The lateral size of free carbon phase (L_a) was then calculated from the intensity ratio of I_D/I_G by Ref. [29]:

$$I_D / I_G = C'(\lambda)*L_a^2 \tag{2}$$

where λ is the wavelength of the laser excitation source, which was 532 nm in this study. The size of the carbon cluster increased from 1.28 nm at 1000 °C to 1.65 nm at 1400 °C, indicating that the free carbon phase was rearranged with increasing pyrolysis temperature, which improved the order degree of the internal structure of the SiAlCN ceramic.

3.2. Resistance−temperature characteristics of the SiAlCN ceramic

The polymer-derived SiAlCN ceramic pyrolyzed at 1000 °C was selected as the sensor head to prepare a temperature sensor, and its resistance−temperature ($R−T$) curve is shown in Fig. 5. The resistance of the SiAlCN ceramic monotonically decreased by approximately two orders of magnitude with increasing temperature from room temperature to 1000 °C, which follows the principle of the negative temperature coefficient of resistance (NTCR). The sensitivity coefficient of the NTCR thermistor (α_T) is another important parameter to evaluate the sensitivity of the sensor, which is defined by the following equation [18,30]:

$$\alpha_T = \left(\frac{1}{\rho}\right)\left(\frac{\partial\rho}{\partial T}\right) = -\frac{B}{T^2} \tag{3}$$

where ρ is the resistivity of the thermistor, T is the temperature, and B is the material constant of the thermistor. The value of B can be calculated by the following equation [6]:

$$B = \frac{ln\left(\frac{R_1}{R_2}\right)}{\left(\frac{1}{T_1} - \frac{1}{T_2}\right)} \tag{4}$$

where R_1 and R_2 are the resistance at temperatures T_1 and T_2, respectively. Generally, T_1 and T_2 are 25 °C and 100 °C. The $B_{25/100°C}$ value of the SiAlCN ceramic calculated by Eq. (4) was 920 K. As the temperature increased from 25 to 1000 °C, the SiAlCN ceramic showed good sensitivity with the sensitivity coefficient of the SiAlCN ceramic changed
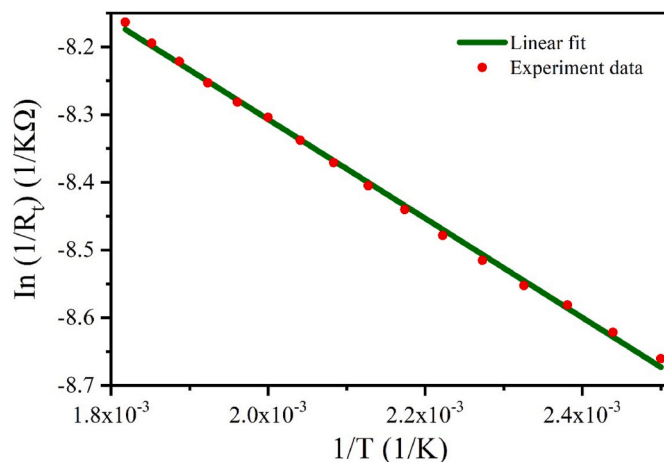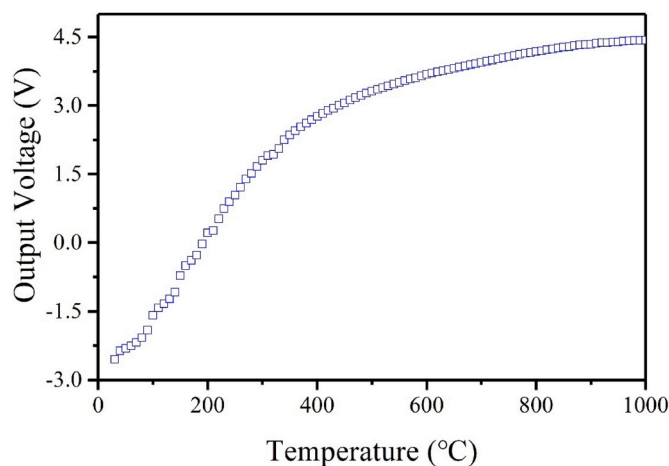

Fig. 7. Output voltage of the SiAlCN sensor as a function of temperature.

from −1.04%/K to −0.07%/K, which is sufficient for the SiAlCN ceramic to be used as sensor material in high-temperature sensing applications.

The thermistor equation Eq. (5) [9]was used to further analyze the resistance−temperature characteristics of the polymer-derived SiAlCN ceramic:

$$ln\frac{1}{R} = C_1\frac{1}{T} - C_2 \tag{5}$$

where C_1 and C_2 are constants, R is the resistance of SiAlCN ceramic, and T is the temperature. The fitted curve of the resistance of the SiAlCN ceramic against the temperature is shown in Fig. 6. The high correlation coefficient of 0.999 indicates that the SiAlCN ceramic followed the thermistor equation very well within the tested temperature range. The constants C_1 and C_2 were determined to be −2044 and −5.74, respectively. The value of C_1 represents the sensitivity of the sensing material. Compared with single-crystal SiC (−1837) [17], the lower C_1 value of the polymer-derived SiAlCN ceramic suggests that the PDC−SiAlCN has higher sensitivity. The linearity, known as the non-linear error, is another important index to describe the static characteristics of a sensor, which is defined by the following equation:

$$\delta = \frac{\Delta Y_{max}}{Y} \times 100\% \tag{6}$$

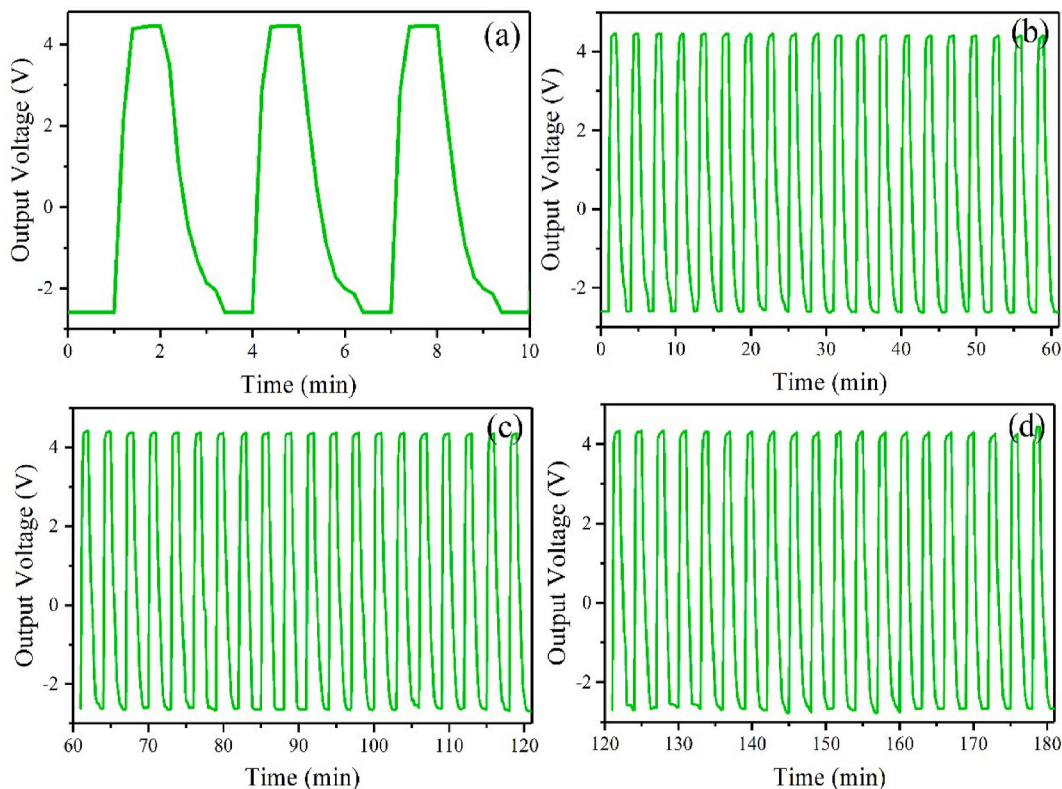where ΔY_{max} is the maximum deviation between the fitted curve and the

Fig. 8. Variation of the output voltage during the cycling test: (a) 1–3 cycles, (b) 1–20 cycles, (c) 21–40 cycles, (d) 41–60 cycles.
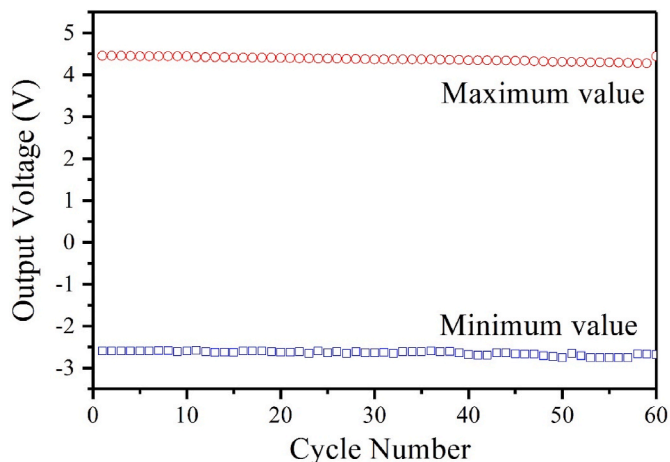

Fig. 9. Maximum and minimum values of the output voltage during the cycling test.

Fig. 10. Comparison of the response rate of the SiAlCN sensor (the blue curve) and a traditional metal-based thermocouple (the black curve). (For interpretation of the references to colour in this figure legend, the reader is referred to the Web version of this article.)

original data, Y is the full-scale output. The δ-value of the SiAlCN ceramic was calculated to be 0.02%, indicating excellent linear characteristics.

3.3. Performances of the SiAlCN temperature sensor

The output voltage of the SiAlCN sensor as a function of temperature is shown in Fig. 7. The output voltage monotonously increased with increasing temperature from room temperature to 1000 °C, indicating stable temperature–voltage conversion.

The variation of the output voltage during 60 heating–cooling cycles is shown in Fig. 8. The first 20 cycles, the middle 20 cycles, and the final 20 cycles are shown in Fig. 7(b)–(d), respectively. All of the output
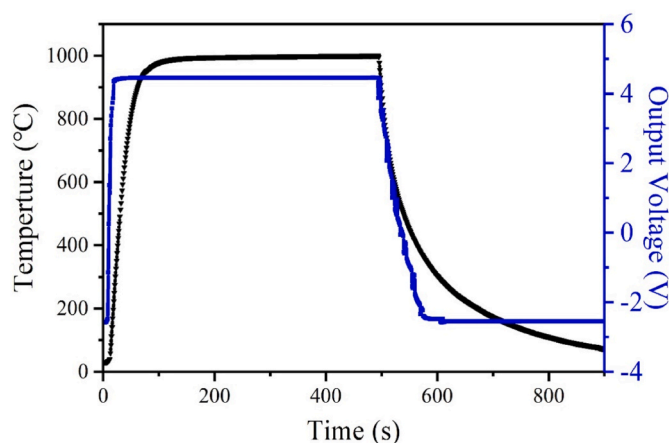
voltage curves exhibited the same variation after 60 cycles. The error ranges of the maximum and minimum values were calculated to be 0.99% and 6.55%, respectively, as shown in Fig. 9. The higher error of the minimum value may be caused by the very large resistance difference between the SiAlCN ceramic and bridge arm at room temperature, leading to lower accuracy. Nevertheless, the prepared SiAlCN temperature sensor showed excellent stability and repeatability.

Comparison of the response rate of the SiAlCN sensor and a traditional thermocouple (the black curve is the variation of the temperature for the thermocouple and the blue curve is the variation of the output voltage for the SiAlCN sensor) is shown in Fig. 10. The SiAlCN sensor and thermocouple were simultaneously placed in a tube furnace
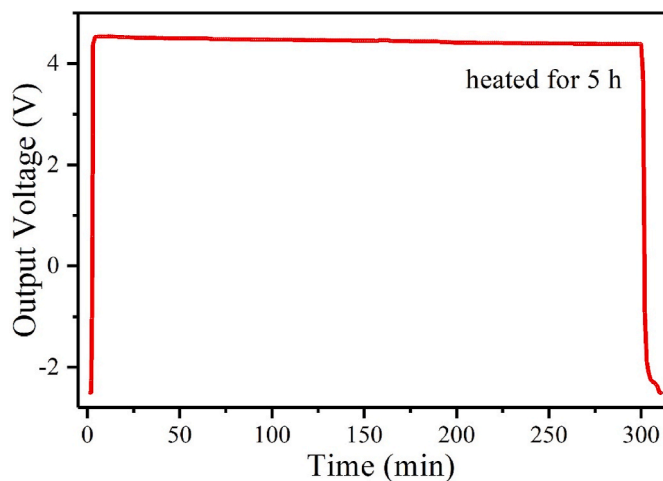
Fig. 11. Output voltage variation of the SiAlCN sensor at 1000 °C for 5 h.

maintained at 1000 °C and taken out after 500 s. The temperature of the thermocouple reached 1000 °C after 90 s, while the output voltage of the SiAlCN sensor reached a plateau immediately after 20 s. During the cooling process, the SiAlCN sensor also showed a faster response rate than the thermocouple, suggesting outstanding sensitivity of the SiAlCN sensor compared with the traditional metal-based thermocouple, which means that the as-prepared SiAlCN sensor can provide a near-instant temperature response.

To measure the stability, the SiAlCN sensor was heated in a tube furnace at 1000 °C for 5 h and the variation of the output voltage is shown in Fig. 11. The output voltage remained stable during the heating period. However, the output voltage slightly decreased (by 3%) after heating for 5 h, which can be attributed to the electricity consumption of the battery in the set-up. The stable output voltage of the SiAlCN sensor suggests its good stability in a high-temperature environment.

4. Conclusion

Polymer-derived SiAlCN ceramics have been synthesized at different temperatures and characterized by XRD, elemental analysis, and Raman spectroscopy. The SiAlCN ceramic pyrolyzed at 1000 °C was used to fabricate a temperature sensor, and its sensing properties, including the resistance−temperature characteristics, repeatability, sensitivity, and stability, were investigated from room temperature to 1000 °C. XRD showed the amorphous character of the SiAlCN ceramic up to 1400 °C, indicating good anti-crystallization ability. The size of the free carbon phase and the order degree of the internal structure gradually increased with increasing pyrolysis temperature.

The SiAlCN ceramic also possessed a NTCR, and the sensitivity co-efficient varied from −1.04%/K to −0.07%/K in the temperature range from 25 to 1000 °C. Multiple heating−cooling cycles demonstrated the excellent repeatability and stability of the SiAlCN sensor. The SiAlCN sensor also showed a faster response rate and a shorter response time than a traditional thermocouple, exhibiting its outstanding sensitivity. Overall, polymer-derived SiAlCN ceramics show great potential for application as sensor materials in high-temperature and harsh environments.

Declaration of competing interest

The authors declare that they have no known competing financial interests or personal relationships that could have appeared to influence the work reported in this paper.

References

[1] Z. Ren, S.B. Mujib, G. Singh, High-temperature properties and applications of Si-based polymer-derived ceramics: a review, Materials 14 (2021) 614.

[2] L.Q. Wang, R. Zhu, G.Z. Li, Temperature and strain compensation for flexible sensors based on thermosensation, Acs. Appl. Mater. Inter. 12 (2020) 1953–1961.

[3] P. Colombo, G. Mera, R. Riedel, G.D. Soraru, Polymer-derived ceramics: 40 Years of research and innovation in advanced ceramics, J. Am. Ceram. Soc. 93 (2010) 1805–1837.

[4] N.R. Nagaiah, J.S. Kapat, L. An, L. Chow, Novel polymer derived ceramic-high temperature heat flux sensor for gas turbine environment, J. Phys. Conf. Ser. 34 (2006) 458–463.

[5] J.B. Casady, W.C. Dillard, R.W. Johnson, U. Rao, A hybrid 6H-SiC temperature sensor operational from 25 °C to 500 °C, IEEE Trans. Compon. Packag. Manuf. A. 19 (1996) 416–422.

[6] A. Feteira, Negative temperature coefficient resistance (NTCR) ceramic thermistors: an industrial perspective, J. Am. Ceram. Soc. 92 (2009) 967–983.

[7] Z.J. Yu, X. Lv, K.W. Mao, Y.J. Yang, A.H. Liu, Role of in-situ formed free carbon on electromagnetic absorption properties of polymer-derived SiC ceramics, J. Adv. Ceram. 9 (2020) 617–628.

[8] Y. Liu, L.A. Liew, R. Luo, L. An, M.L. Dunn, V.M. Bright, J.W. Daily, R. Raj, Application of microforging to SiCN MEMS fabrication, Sensor. Actuat. A-Phys. 95 (2002) 143–151.

[9] R. Zhao, G. Shao, Y.J. Cao, L.N. An, C.Y. Xu, Temperature sensor made of polymer-derived ceramics for high-temperature applications, Sensor. Actuat. A-Phys. 219 (2014) 58–64.

[10] W. Zhao, G. Shao, M. Jiang, B. Zhao, H. Wang, D. Chen, H. Xu, X. Li, R. Zhang, L. An, Ultralight polymer-derived ceramic aerogels with wide bandwidth and effective electromagnetic absorption properties, J. Eur. Ceram. Soc. 37 (2017) 3973–3980.

[11] H.R. Hong, W. Liu, M. Zhang, Y.G. Wang, Y. Chen, Uniformly dispersed nano-crystallite graphite in a silicon-oxygen-carbon matrix for high rate performance lithium-ion batteries, J. Alloys Compd. 857 (2021) 157476.

[12] R. Riedel, L.M. Ruswisch, L. An, R. Raj, Amorphous silicoboron carbonitride ceramic with very high viscosity at temperatures above 1500 degrees C, J. Am. Ceram. Soc. 81 (1998) 3341–3344.

[13] Y.G. Wang, Y. Fan, L.G. Zhang, W.G. Zhang, L.A. An, Polymer-derived SiAlCN ceramics resist oxidation at 1400 °C, Scripta Mater. 55 (2006) 295–297.

[14] Y.X. Yu, Q.F. Huang, S. Rhodes, J.Y. Fang, L.N. An, SiCNO-GO composites with the negative temperature coefficient of resistance for high-temperature sensor applications, J. Am. Ceram. Soc. 100 (2017) 592–601.

[15] G. Shao, J.P. Jiang, M.J. Jiang, J. Su, W. Liu, H.L. Wang, H.L. Xu, H.X. Lit, R. Zhang, Polymer-derived SiBCN ceramic pressure sensor with excellent sensing performance, J. Adv. Ceram. 9 (2020) 374–379.

[16] H.D. Batha, P.E. Carroll, Unicrystalline silicon carbide thermistor, IEEE Trans. Compon. Parts 11 (2003) 129–134.

[17] L. An, W. Xu, S. Rajagopalan, C. Wang, H. Wang, Y. Fan, L. Zhang, D. Jiang, J. Kapat, L. Chow, Carbon-nanotube-reinforced polymer-derived ceramic composites, Adv. Mater. 16 (2004) 2036–2040.

[18] M.N. Muralidharan, P.R. Rohini, E.K. Sunny, K.R. Dayas, A. Seema, Effect of Cu and Fe addition on electrical properties of Ni-Mn-Co-O NTC thermistor compositions, Ceram. Int. 38 (2012) 6481–6486.

[19] X.W. Yin, L. Kong, L.T. Zhang, L.F. Cheng, N. Travitzky, P. Greil, Electromagnetic properties of Si-C-N based ceramics and composites, Int. Mater. Rev. 59 (2014) 326–355.

[20] Y.G. Wang, L.N. An, Y. Fan, L.G. Zhang, S. Burton, Z.H. Gan, Oxidation of polymer-derived SiAlCN ceramics, J. Am. Ceram. Soc. 88 (2005) 3075–3080.

[21] Y.D. Yu, J.P. Li, J.H. Niu, F.J. Yi, S.H. Meng, The stability and repeatability of high temperature electrical properties of SiAlCN ceramic sensor heads, Ceram. Int. 45 (2019) 7588–7593.

[22] C. Ma, G. Shao, J.P. Jiang, W.L. Liu, H.L. Wang, H.X. Lu, B.B. Fan, X.J. Li, R. Zhang, L.N. An, Temperature dependent AC electric conduction of polymer-derived SiAlCN ceramics, Ceram. Int. 44 (2018) 8461–8466.

[23] N. Janakiraman, F. Aldinger, Fabrication and characterization of fully dense Si-C-N ceramics from a poly (ureamethylvinyl) silazane precursor, J. Eur. Ceram. Soc. 29 (2009) 163–173.

[24] Y.H. Chen, X.P. Yang, Y.J. Cao, L.A. An, Effect of pyrolysis temperature on the electric conductivity of polymer-derived silicoboron carbonitride, J. Eur. Ceram. Soc. 34 (2014) 2163–2167.

[25] A.C. Ferrari, J. Robertson, Interpretation of Raman spectra of disordered and amorphous carbon, Phys. Rev. B 61 (2000) 14095–14107.

[26] A.C. Ferrari, J. Robertson, Resonant Raman spectroscopy of disordered, amorphous, and diamondlike carbon, Phys. Rev. B 64 (2001), 075414.

[27] A. Sadezky, H. Muckenhuber, H. Grothe, R. Niessner, U. Poschl, Raman micro spectroscopy of soot and related carbonaceous materials: spectral analysis and structural information, Carbon 43 (2005) 1731–1742.

[28] E.H. Martins Ferreira, M.V.O. Moutinho, F. Stavale, M.M. Lucchese, R.B. Capaz, C. A. Achete, A. Jorio, Evolution of the Raman spectra from single-, few-, and many-layer graphene with increasing disorder, Phys. Rev. B 82 (2010) 125429.

[29] G.A. Zickler, B. Smarsly, N. Gierlinger, H. Peterlik, O. Paris, A reconsideration of the relationship between the crystallite size L-a of carbons determined by X-ray diffraction and Raman spectroscopy, Carbon 44 (2006) 3239–3246.

[30] A. Feltz, W. Polzl, Spinel forming ceramics of the system FexNiyMn$_3$-x-yO$_4$ for high temperature NTC thermistor applications, J. Eur. Ceram. Soc. 20 (2000) 2353–2366.